



# Superhydrophobic photothermal icephobic surfaces based on candle soot

Shuwang Wu<sup>a,b</sup>, Yingjie Du<sup>a</sup>, Yousif Alsaied<sup>a</sup>, Dong Wu<sup>a</sup>, Mutian Hua<sup>a</sup>, Yichen Yan<sup>a</sup>, Bowen Yao<sup>a,b</sup>, Yanfei Ma<sup>a</sup>, Xinyuan Zhu<sup>b,1</sup>, and Ximin He<sup>a,1</sup>

<sup>a</sup>Department of Materials Science and Engineering, University of California, Los Angeles, CA 90095; and <sup>b</sup>School of Chemistry and Chemical Engineering, State Key Laboratory of Metal Matrix Composites, Shanghai Jiao Tong University, Shanghai 200240, China

Edited by David A. Weitz, Harvard University, Cambridge, MA, and approved April 6, 2020 (received for review February 2, 2020)

Ice accumulation causes various problems in our daily life for human society. The daunting challenges in ice prevention and removal call for novel efficient antiicing strategies. Recently, photothermal materials have gained attention for creating icephobic surfaces owing to their merits of energy conservation and environmental friendliness. However, it is always challenging to get an ideal photothermal material which is cheap, easily fabricating, and highly photothermally efficient. Here, we demonstrate a low-cost, high-efficiency superhydrophobic photothermal surface, uniquely based on inexpensive commonly seen candle soot. It consists of three components: candle soot, silica shell, and polydimethylsiloxane (PDMS) brushes. The candle soot provides hierarchical nano/microstructures and photothermal ability, the silica shell strengthens the hierarchical candle soot, and the grafted low-surface-energy PDMS brushes endow the surface with superhydrophobicity. Upon illumination under 1 sun, the surface temperature can increase by 53 °C, so that no ice can form at an environmental temperature as low as −50 °C and it can also rapidly melt the accumulated frost and ice in 300 s. The superhydrophobicity enables the melted water to slide away immediately, leaving a clean and dry surface. The surface can also self-clean, which further enhances its effectiveness by removing dust and other contaminants which absorb and scatter sunlight. In addition, after oxygen plasma treatment, the surface can restore superhydrophobicity with sunlight illumination. The presented icephobic surface shows great potential and broad impacts owing to its inexpensive component materials, simplicity, ecofriendliness, and high energy efficiency.

candle soot | superhydrophobic | photothermal | icephobic | self-cleaning

Icing is a ubiquitous and unavoidable phenomenon that occurs in nature through various means such as frosting, condensation freezing, and frozen rain (1). It has been a long-standing problem and disruption in human society, as it impacts many aspects of our daily life. For instance, ice formation and accumulation can cause mechanical failures in vehicles and aircrafts; structural damage can be found in wind turbines, residential houses, and power lines; optical malfunction has also been found in telescope lens and windows (2–7). Icing also has a long history of creating life-threatening hazards ranging from slipping accidents to traffic collisions. All these icing-induced problems present many challenges and great demands for developing antiicing strategies (8, 9).

Traditional antiicing strategies include heating, as well as chemical and mechanical deicing (8, 10). Unfortunately, they all suffer from being energy-intensive, low efficiency, and environmentally unfriendly. Specifically, compared with the chemical and mechanical methods, heating deicing strategies still are one of the most practical methods. However, the current heating methods need complex energy supply systems and are highly energy inefficient (6, 8). Meanwhile, the recent advancement of the understanding of icing process is also beneficial for the development of new antiicing methods. Icing process usually includes different stages such as condensation, nucleation, and accumulation. More recently, a variety of strategies have been

proposed to design icephobic materials through surface modification and targeting different stages of the icing process. For example, superhydrophobic surfaces with nano/microstructures can remove water droplets during the condensation stage, to delay ice nucleation and decrease ice accumulation (11). Anti-freezing materials with ion-rich polymer coating have been developed to regulate interfacial water and thus delay the nucleation of ice (12). Another class of materials has been designed to target ice removal after freezing, by creating liquid or organic lubricant-impregnated surfaces to reduce ice adhesion (13–15). Although these efforts have contributed to the development of antiicing surfaces from different perspectives, a variety of drawbacks and challenges still remain. For instance, lubricant-impregnated surfaces are unsuitable for long-term usage due to the degradation of lubricant via cloaking, evaporation, or capillary wicking (16). For superhydrophobic surfaces, ice can interlock with the hierarchical structures and increase adhesion strength with the material surface (17, 18). If deicing with mechanical methods (e.g., shoveling, rubbing, abrasion), the material surface structures can be destroyed, so as the antiicing functions, due to the physical contact and great impact on the surface (18). The noncontact remote illumination method is obviously mild and long-lasting.

Creating icephobic surfaces using photothermal effect has drawn increasing attention due to their attractive energy conservation

## Significance

Here cheap candle soot is utilized to make superhydrophobic photothermal icephobic surfaces. The candle soot provides the hierarchical structure for superhydrophobicity; meanwhile, sunlight can be trapped in the hierarchical structure to enhance the light absorption leading to a high photothermal efficiency. The superhydrophobicity can help maintain the excellent photothermal performance. Firstly, the superhydrophobic candle soot surface can remove the melted water immediately leaving a dry surface, which avoids the reflectance and thermal mass of melted water and thus reduces the heat loss. Secondly, the surface is capable of self-cleaning; dust and other contaminants can be washed away by rain or melted water to prevent the blocking and scattering of sunlight, highly benefiting the maintaining of long-term high photothermal efficiency.

Author contributions: S.W. and X.H. designed research; S.W., Y.D., Y.A., D.W., and M.H. performed research; S.W., Y.D., Y.A., D.W., Y.Y., B.Y., Y.M., and X.H. contributed new reagents/analytic tools; S.W., X.Z., and X.H. analyzed data; and S.W., Y.D., Y.A., X.Z., and X.H. wrote the paper.

The authors declare no competing interest.

This article is a PNAS Direct Submission.

Published under the PNAS license.

<sup>1</sup>To whom correspondence may be addressed. Email: xyzhu@sjtu.edu.cn or ximinhe@ucla.edu.

This article contains supporting information online at <https://www.pnas.org/lookup/suppl/doi:10.1073/pnas.2001972117/-DCSupplemental>.

by utilizing ample environmental light and environmental friendliness without harmful chemicals (19–23). Recently, it has been shown that plasmonic (21, 24, 25), magnetic particles (20, 26), and carbon nanomaterials (26, 27) can be utilized in photothermal surfaces to generate heat from photo/solar energy and melt accumulated ice. However, there are limitations and remaining challenges. Firstly, these materials are usually costly and/or difficult to fabricate, involving sophisticated chemical syntheses and deposition technologies. For example, carbon nanomaterials cannot be made as coatings without adding polymer binders. Secondly, with current strategies, the melted water remains on the surface, which can freeze again in the absence of continuous illumination. Furthermore, the remaining melted water will greatly decrease the photothermal efficiency due to water's high reflectance of sunlight and inherently high specific heat capacity. Therefore, it is crucial to remove the melted water to obtain a clean and dry surface. Thirdly, in outdoor applications, the surface can be easily covered with dust and other contaminants which will block sunlight, resulting in the inefficient use of solar energy (28). It is therefore highly desirable to develop new strategies for multifunctional surfaces to simultaneously melt ice and remove water, along with other contaminants, by utilizing the photothermal effect and superhydrophobicity.

We note that candle soot has the potential to be used in fabricating such multifunctional surfaces, as it naturally possesses two desirable features, structurally and physically. Structurally, incomplete combustion naturally forms nearly perfect hierarchical structure from nanoscale carbon material assemblies. Such a hierarchical structure makes the soot deposited on substrates an ideal superamphiphobic coating (29). Physically, its black color with excellent photothermal conversion effect allows it to function as a photothermal material (30). Uniquely within this natural hierarchical photothermal material, these two factors mutually enhance each other. The hierarchical structure of candle soot is not only necessary for superhydrophobicity, it is also beneficial for photothermal conversion because of the sunlight trapping via multiple internal reflections. Moreover, the superhydrophobicity can further improve the photothermal performance in two aspects: firstly, candle soot surface can remove the melted water immediately leaving a dry surface; thus,

the reflectance and thermal mass of melted water can be avoided to greatly reduce the heat loss. Secondly, dust and other contaminants can be easily washed away by the melted water or rain leaving a clean surface, which prevents the blocking and scattering of sunlight and thus highly benefits maintaining the long-term high photothermal efficiency. Overall, based on this mechanism rooted from these two structural and physical properties of candle soot, we have successfully demonstrated its use as an inexpensive and highly efficient superhydrophobic photothermal coating, capable of removing condensate drops, frost, and ice. Under 1-sun illumination, no ice can form the surfaces when the environmental temperature is as low as  $-50\text{ }^{\circ}\text{C}$ , significantly lower than the freezing temperatures that state-of-the-art methods can achieve. Such a high-performance antiicing surface features self-cleaning, self-healing upon illumination, and high durability.

## Results

Candle soot was facily deposited onto a glass slide by simply holding it above the candle flame, as shown in Fig. 1A. The bare candle soot layer (termed as CS) was very fragile, because there were only weak physical interactions between the CS particles and the glass, as depicted in *SI Appendix, Fig. S1*. To strengthen the CS layer to make the coating more robust, a silica shell was coated onto the soot particles (termed as SCS) via chemical vapor deposition (CVD) of tetraethoxysilane (TEOS) (*SI Appendix, Fig. S2*). Finally, polydimethylsiloxane (PDMS) brushes were grafted onto the silica shell under UV light (*SI Appendix, Fig. S3*, termed as PSCS) (31–33) to introduce a superhydrophobic layer, instead of the more typical fluorine which is considered an environmental hazard (34). Thus, the coating consists of three components—CS particles, silica shell, and PDMS brushes (Fig. 1B). Each of them provides a different function: the CS particles generate heat under sunlight illumination, the silica shell strengthens the coating to be more robust, and the PDMS brushes endow the coating with superhydrophobicity. The proposed icephobic surface possesses both photothermal and superhydrophobic properties: When illuminated by sunlight, the accumulated ice can melt from the heat generated by the soot layer via the photothermal effect, and meanwhile the melted water can roll off easily because of the superhydrophobic top layer (Fig. 1C and D).

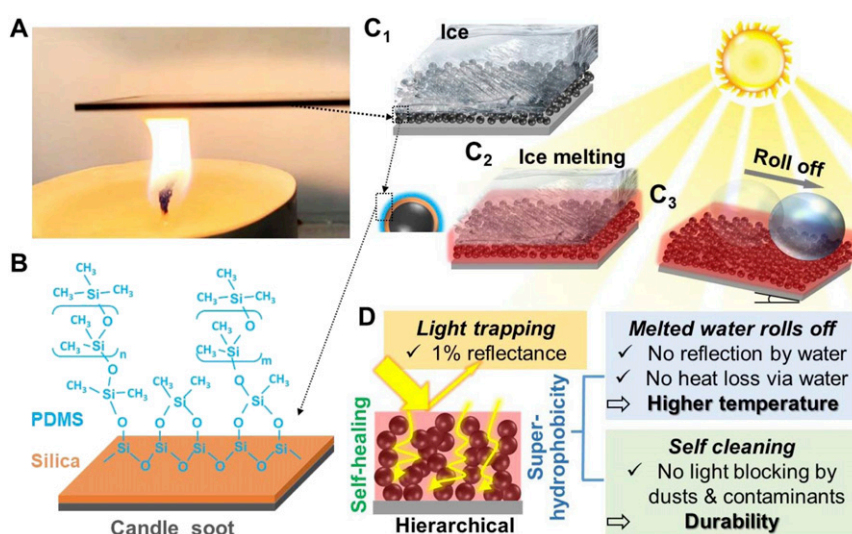


**Fig. 1.** Schematic of the icephobic surface and fabrication process. (A) Deposition of CS onto glass slide held above the candle flame. (B) Structures of the soot particles after coated with silica shell and PDMS brushes subsequently, prepared as *SI Appendix, Fig. S1* depicts. (C) Working mechanism of the proposed icephobic surface. Under the illumination of sunlight, the accumulated ice on the surface ( $C_1$ ) can melt due to the heat generated via photothermal effect ( $C_2$ ), and the melted water can roll off on the tilt surface ( $C_3$ ). (D) The hierarchical structures endow the surfaces with abilities of light trapping and superhydrophobicity.

When the glass slide is held above the candle flame, it acts as a barrier between the flame and oxygen, resulting in incomplete combustion and generates carbon nanoparticles (29, 34). These carbon nanoparticles coagulate and agglomerate to form the CS layer. Fig. 2  $A_1$  and  $A_2$  show the morphology of bare CS layer which consists of interconnected carbon particles with a typical diameter of 30–40 nm. This loose, fractal-like soot layer has micronanoscale roughness. Combined with the low surface energy of the carbon surfaces, the CS layer is inherently superhydrophobic. When a water droplet was placed on the CS surface, the static contact angle was measured to be  $161 \pm 1^\circ$  (Fig. 2 $A_3$ ) and the droplet was observed to slide off easily (sliding angle  $\sim 1^\circ$ ). However, due to the weak physical interaction between the soot nanoparticles, the CS layer was too fragile to withstand the impact force of the sliding water droplet. The layer can be destroyed after a few droplets (*SI Appendix, Fig. S4*). To strengthen the CS layer, a silica shell was coated onto the soot particles using CVD method (*SI Appendix, Fig. S2*). The CVD process occurred through the hydrolysis and condensation of TEOS catalyzed by hydrochloric acid (*SI Appendix, Fig. S2*) (34, 35). After being coated with silica, the morphology was similar to that of the bare soot layer (Fig.  $B_1$ ), while the diameter of particles increased to 100 nm (Fig.  $B_2$ ), indicating the formation of silica shells. The silica that wrapped around the interconnected soot particles formed strong interparticle bonding, which significantly enhanced the stability and robustness of the bare soot coating (Fig.  $B_2$ ). However, due to the hydrophilic nature of silica, the SCS layer is not hydrophobic (Fig.  $B_3$ ) (34). PDMS was then grafted onto the silica shell by ultraviolet (UV) illumination. The morphology remained unchanged at the micrometer scale after grafting PDMS (Fig.  $2C_1$ ). However, scanning electron microscope (SEM) images taken at higher magnifications showed that the edges between particles were smoother than before grafting. This indicated that the PDMS was successfully grafted on the silica (Fig.  $2C_2$ ). With the PDMS-brush surface, the contact angle increased to  $163 \pm 1^\circ$  (Fig.  $2C_3$ ). At the same time, water droplets rolled away easily with a sliding angle smaller than  $5^\circ$ .

The thickness of CS can be tuned by simply varying the deposition time. Fig. 3  $A$ – $C$  show the cross-section of soot layers with the thickness of 1.5, 5.1, and 30.0  $\mu\text{m}$ , respectively. All of the soot layers have homogeneous porous structures. Temperature increases ( $\Delta T$ ) on the coating layer have been measured under 1 sun ( $1 \text{ kW/m}^2$ ). Fig. 3 $D$  (*Inset*) shows the  $\Delta T$  increases greatly with illumination time and reaches a maximum value of  $50^\circ\text{C}$  after 300 s. With 1-sun illumination, the CS is highly competitive in temperature increase  $\Delta T$  and heating rate ( $0.17^\circ\text{C/s}$ ), comparing with previous outstanding photothermal icephobic surfaces (19, 21). Meanwhile,  $\Delta T$  increases with soot layer thickness (Fig. 3 $D$ ), reaching a plateau as the thickness is greater than  $\sim 10 \mu\text{m}$ . It is possible that this limit is determined by the sun light penetration depth. Since the multifunctional coating has hybrid interfaces with silica and PDMS layers on the soot for high robustness and hydrophobicity, we have investigated whether the silica shell and PDMS brushes affect the photothermal efficiency. As shown in Fig. 3 $E$ , after illuminated under 1 sun for 300 s, the  $\Delta T$  of CS, SCS, and PSCS are  $53.3$ ,  $53.2$ , and  $53.3^\circ\text{C}$ , respectively, indicating that the silica shell and PDMS brushes have little impact on the photothermal efficiency (36). Furthermore, the  $\Delta T$  of PSCS has been measured after exposure to different light intensities. The  $\Delta T$  increases from  $20^\circ\text{C}$  to  $53^\circ\text{C}$  and  $73^\circ\text{C}$  as the light intensity increases from 0.5 sun to 1 sun and 1.5 sun (Fig. 3 $F$  and *SI Appendix, Fig. S5*). The infrared images also indicate that the temperature of PSCS is uniform across the entire surface. Importantly, compared with flat surfaces which strongly reflect light, the CS surfaces with the hierarchical structures have nanoscale feature size, which is smaller than the wavelength of sunlight and known for effective light trapping. Thus, the light gets trapped in the hierarchical structures, resulting in multiple internal reflections until absorbed completely (37). The mechanism is verified by experiment comparing various black surfaces with different nano/microstructures. When sunlight falls on the PSCS surface,  $<1\%$  of the sunlight is reflected and scattered as measured experimentally (*SI Appendix, Fig. S6*). This remarkable absorption contributes greatly to the high photothermal efficiency of the CS coating.

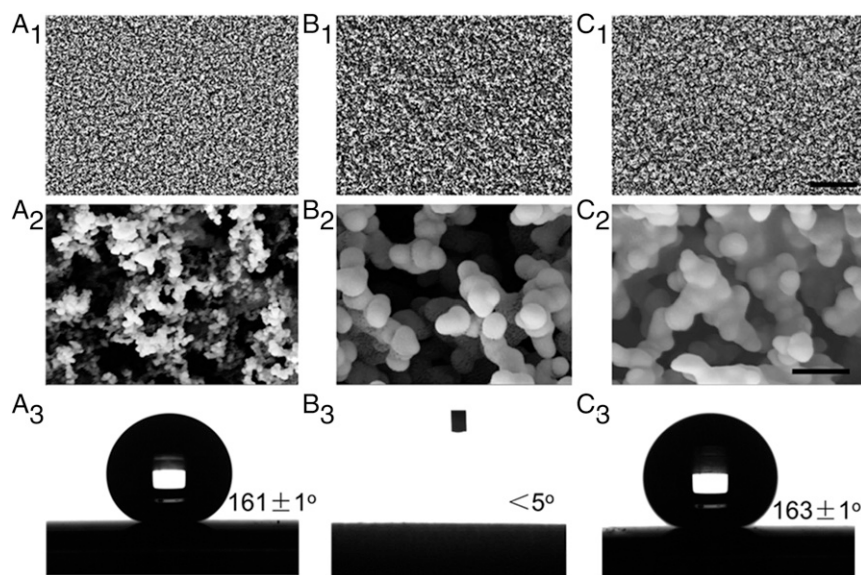


**Fig. 2.** Morphology and wettability of the surfaces. ( $A_1$  and  $A_2$ ) SEM images of CS layer. ( $A_3$ ) Water contact angle of the CS surface. ( $B_1$  and  $B_2$ ) SEM images of SCS. ( $B_3$ ) Water contact angle of SCS surface. ( $C_1$  and  $C_2$ ) SEM images of the structures after PSCS. ( $C_3$ ) Water contact angle of the PSCS surface. (Scale bars:  $a_1$ ,  $b_1$ , and  $c_1$ , 5  $\mu\text{m}$ ; Scale bars:  $a_2$ ,  $b_2$ , and  $c_2$ , 200 nm.)

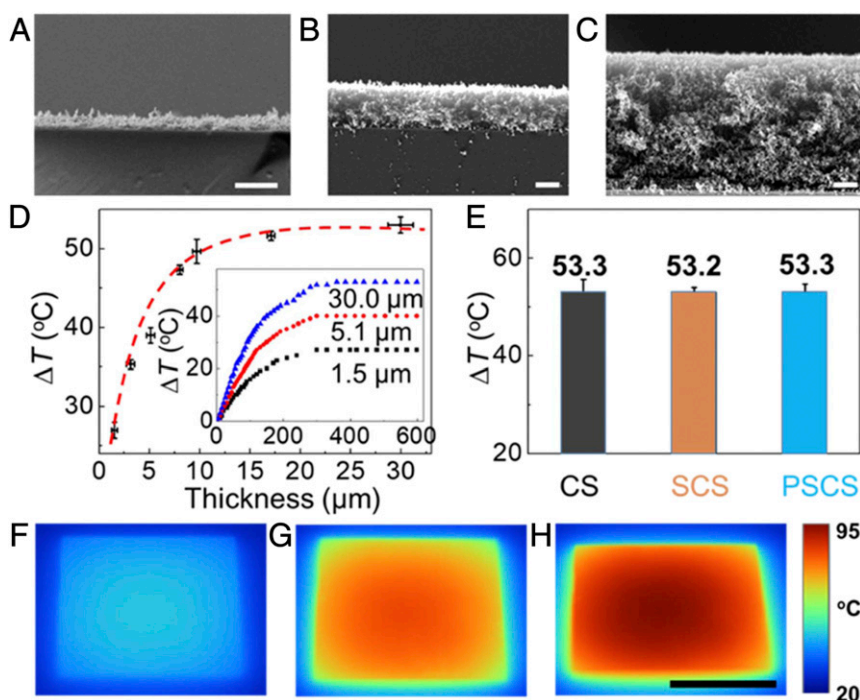


**Fig. 3.** Photothermal properties of the deposited CS layers. (A–C) Cross-section SEM images of CS with thickness of 1.5  $\mu\text{m}$  (A), 5.1  $\mu\text{m}$  (B), and 30  $\mu\text{m}$  (C), respectively. (D) Temperature increases ( $\Delta T$ ) of CS with different thickness under 1 sun. (Inset) Profiles of  $\Delta T$  as the illumination time under 1 sun. (E) Temperature increases ( $\Delta T$ ) of bare CS, SCS, and PSCS. (F) Infrared camera images of PSCS under 0.5 sun ( $f_1$ ), 1.0 sun ( $f_2$ ), and 1.5 sun ( $f_3$ ), respectively. The thickness of CS, SCS, and PSCS are 30.0  $\mu\text{m}$  and the temperatures were measured after illumination under 1 sun for 300 s. (Scale bars: A, B, and C, 2  $\mu\text{m}$ ; Scale bars: F, G, and H, 1 cm.)

Superhydrophobic surfaces exhibit icephobicity by removing condensed water before it can freeze (38). As shown in *SI Appendix, Fig. S7 (Movie S1)*, during condensation, water droplets coalesced and jumped off, being propelled by the released surface energy during droplet coalescence, as commonly observed in reported superhydrophobic surfaces (39). At the same time, it is known that with the superhydrophobic surfaces, the small contact area between substrate and water droplet inhibits ice formation with fewer nucleation sites (40). As Fig. 2  $B_3$  and  $C_3$  have shown, the SCS surface was hydrophilic and after grafting with PDMS, the PSCS became superhydrophobic. When a droplet was placed on the PSCS surface during the icing process, the surface remained superhydrophobic even after the water droplet froze (*SI Appendix, Fig. S8* and ref. 41).

In many situations where the entire surface is covered by frost or ice in subzero temperature environments, the typical solutions to remove the accumulated ice are mechanical methods, which involve great physical contact and impact on the surface. However, as mentioned earlier, this can destroy the surface structure and anti-icing function of the material. Using sunlight as a source to melt ice can minimize the damage of these hierarchical structures. Compared with compact and transparent bulk ice, frost is porous and fractal and reflects and scatters sunlight more strongly, making it challenging to melt frost using sunlight. Here, we systematically studied the abilities of SCS and PSCS for melting frost and ice, respectively, with sunlight illumination. First, frost was allowed to accumulate on SCS and PSCS surfaces as they were cooled for 2 h at  $-30^\circ\text{C}$ . Next, both surfaces were illuminated with 1 sun. On the PSCS surface, the frost started melting after being illuminated for 60 s and melted water formed water droplets on the surface (Fig. 4 $A_1$ ). By contrast, the SCS surface required a much longer time (240 s) to melt the same amount of frost (Fig. 4 $A_2$ ). Furthermore, noticeably on the SCS

surface the melted water remained on the surface, while the PSCS surface was nearly free of water, and the small amount of remaining melted water on it bulges up into tiny droplets (*Movie S2*), which can readily roll off the surface (*Movie S2*). Furthermore, the ice-melting ability of SCS and PSCS was tested. Fig. 4B shows the melting process of ice on PSCS and SCS surfaces. Within 720 s of illumination, all of the ice on the PSCS surface melted and the water slipped onto the stage (Fig. 4 $B_1$  and *Movie S3*). In contrast, only a portion of the ice melted on the SCS surface with the same illumination time (Fig. 4 $B_2$  and *Movie S3*). On the SCS surface, the remaining melted water strongly decreased the photothermal efficiency (infrared images of SCS and PSCS in Fig. 4 and *SI Appendix, Fig. S9* and *Movie S4*) due to the strong reflection and the large thermal mass of water (specific thermal captivity/capacity, 4.2 kJ/(kg·K) of water vs. 1.0 kJ/(kg·K) of air on our dry PSCS surface) as an undesirable heat sink during the melting process. This resulted in much longer time to melt the frost on SCS surface. By contrast, without the melted water remaining on the surface, the PSCS surface had quickly raised surface temperature, nearly 10 $\times$  higher than the SCS surface temperature (8.5 vs. 0.9  $^\circ\text{C}$ ), and effectively shortened the defrosting time for  $\sim 66\%$  (120 vs. 240 s). As for durability, compared with the mechanical deicing methods, melting ice with photothermal effect causes no damage to the hierarchical structures and shows excellent stability after 20 icing–deicing cycles (*SI Appendix, Fig. S10*).

Furthermore, not only is the photothermal surface not prone to damage using this mild remote illumination method, the PSCS surface can even self-recover its superhydrophobicity capability, simply under light illumination (*SI Appendix, Fig. S11*). When the PSCS surfaces were exposed to oxygen plasma, polar groups were introduced onto surfaces (42); so that the surface became superhydrophilic with contact angle lower than  $10^\circ$ . After illuminated

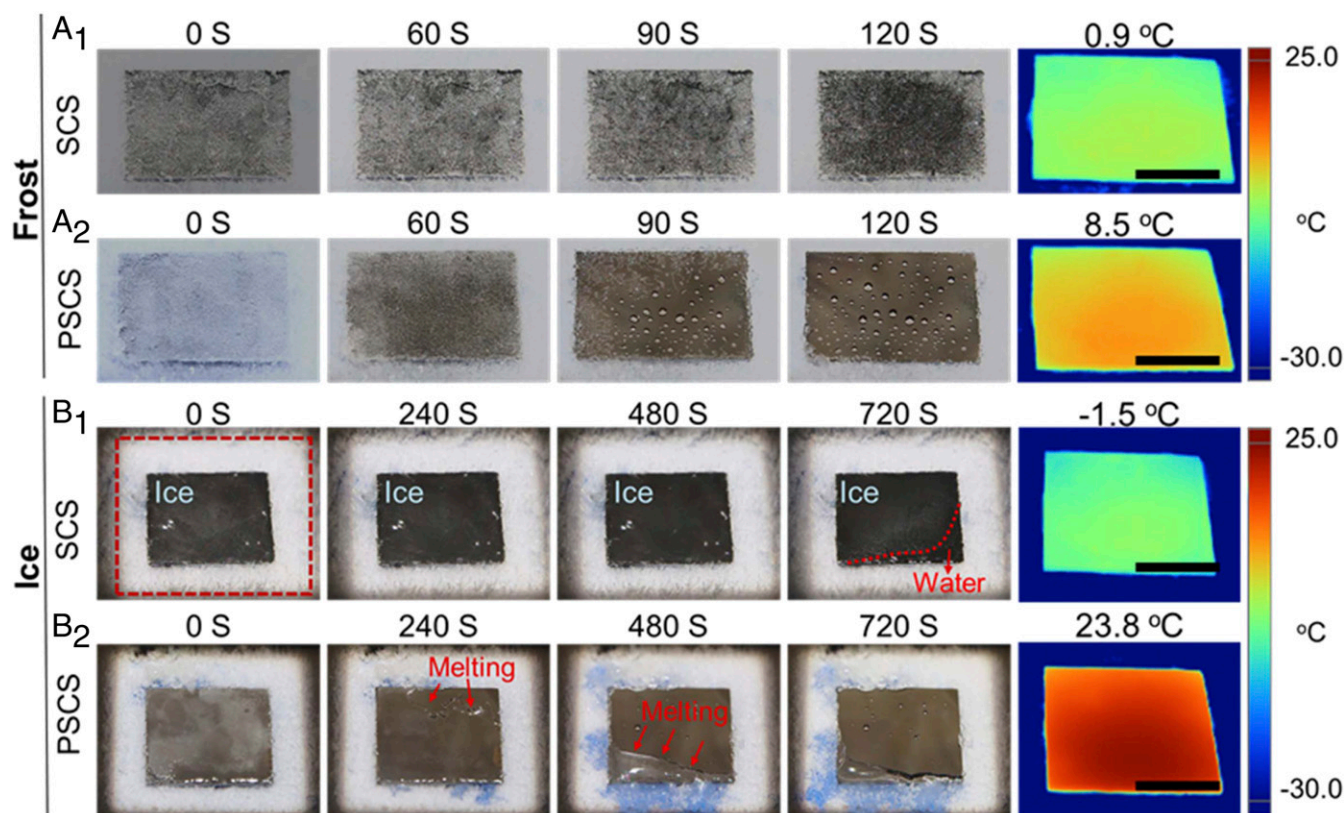


**Fig. 4.** Photothermally induced melting of frost and ice on SCS and PSCS surfaces under 1-sun illumination. (A) The melting of frost on the superhydrophilic SCS surface ( $A_1$ ) and superhydrophobic PSCS surface ( $A_2$ ). (B) The melting of ice on the superhydrophilic SCS surfaces ( $B_1$ ) and superhydrophobic PSCS surface ( $B_2$ ). (Scale bars: 1 cm.)

under 1 sun for 1 h, the surface restored superhydrophobicity with contact angle higher than  $150^\circ$ , which might be due to the rotation of the PDMS brushes triggered by the heat generated via the photothermal effect under 1 sun (43). The healed PSCS surface showed self-cleaning properties owing to its unique superhydrophobic feature, which can take away the sands, scraps of paper, and other contaminants (Fig. 5 A and B). In real outdoor applications, this self-cleaning property is critical for the photothermal efficiency because the contaminants can block and scatter the sunlight (28). As shown in Fig. 5 C and D, when the SCS and PSCS surfaces were covered with sands, the temperature could be increased by only  $14.5^\circ\text{C}$ . However, on the PSCS surface, the temperature was heated up by  $50^\circ\text{C}$  again, as soon as the sands were taken away easily by water droplets.

## Conclusion

Here we demonstrated that CS can be used to build photothermal anti-icing coating, by providing the hierarchical structures and generating heat with solar illumination. The coating exhibited good mechanical robustness owing to the silica shell and superhydrophobicity by grafting PDMS brushes. It was demonstrated that the temperature can be rapidly increased by  $53^\circ\text{C}$  with illumination intensity of 1 sun. The hierarchical structure is extremely important for the photothermal performance because sunlight can be reflected multiply in the nano-/microporous structure, which effectively enhances the adsorption. During melting, the accumulated frost and ice on PSCS surface can be melted faster than on the hydrophilic SCS surfaces, due to the easy roll-off of water droplet, leaving almost no remaining water. The remaining water can greatly reflect and adsorb sunlight, causing huge heat loss; hence, the PSCS surface

has much better photothermal performance with lower freezing temperature and shorter melting time. Meanwhile, the superhydrophobicity also endows the surface with self-cleaning ability. Rain and the melted water will slide away and clean the contaminants like dust preventing blocking and scattering of sun light which guarantees long-term icephobicity with high photothermal efficiency. Compared with traditional mechanical deicing methods, the melting induced by photothermal effect can reduce the damage the hierarchical structures during the deicing process. PSCS surfaces can also restore the superhydrophobicity with the heat generated by the photothermal effect under 1 sun. In conclusion, the PSCS surfaces show great potential for making icephobic surfaces because of the inexpensive component materials, simplicity, ecofriendliness, and energy efficiency.

## Materials and Methods

**Materials.** TEOS (Sigma-Aldrich, 98%), hydrochloric acid (ACS reagent, 37%), PDMS (Sylgard 184), hexane (Sigma-Aldrich, 95%), milli-Q water. All of the materials were used without further purification.

**Fabrication of Icephobic Surface.** Firstly, the glass slides were held above the flame to deposit the CS layer. Then the soot-coated glass slides were placed in a desiccator in which two beakers containing about 2 mL of TEOS and hydrochloric acid, respectively (SI Appendix, Fig. S2). The desiccator was evacuated overnight to proceed with CVD of TEOS forming the SCS. To graft the PDMS brushes, the SCS was immersed in 2% PDMS-hexane solution firstly, then put the samples into UV hood for 10 min (UV power: 400 W, 320–390 nm). The unreacted PDMS was washed away by plenty of hexane.

**Characterizations.** The morphology was observed with a Supra 40VP SEM. To measure the contact angle,  $3\ \mu\text{L}$  of pure water was put on the surfaces and recorded with DSA 100. Sun simulator was used to provide light source and

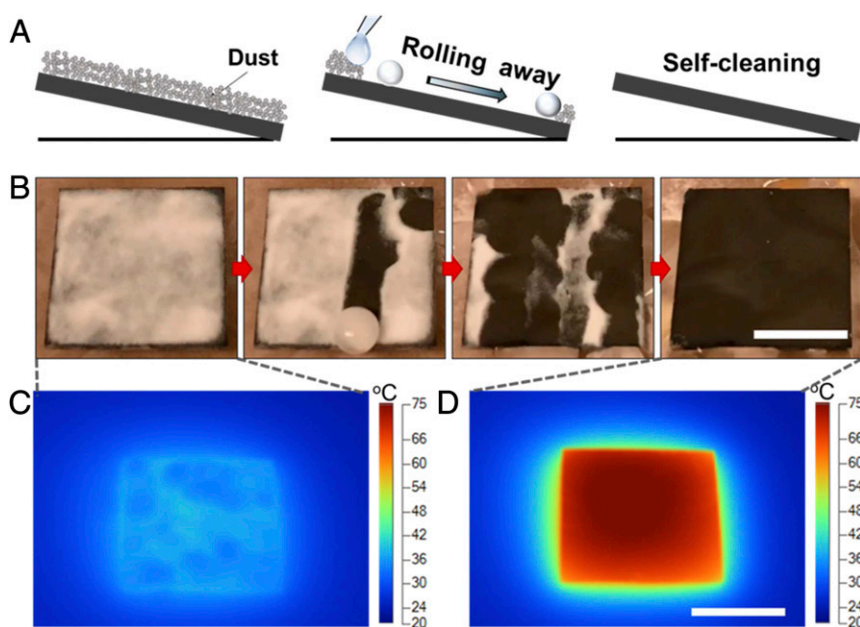


**Fig. 5.** The self-cleaning performance and temperature with and without dust under 1-sun illumination. (A and B) The schematic and experiment of the self-cleaning process. Sands were used to demonstrate the self-cleaning property. The sands were easily taking away by the rolling water droplet. (C and D) Infrared camera images of the PSCS under 1 sun before (C) and after (D) self-cleaning. (Scale bars: 1 cm.)

the temperature was monitored and recorded with a thermocouple. An infrared camera (Fluke XV) was used to map the temperature of the samples.

**Anticing Experiments.** These experiments were proceeded in a homemade system (SI Appendix, Fig. S12). The condensation process was observed via a microscope (Teslong, 4.3-mm-diameter Visual Scope Camera). The freezing and melting processes were recorded with a digital camera.

**Data Availability.** All data needed to evaluate the conclusions of the paper are present in the main text, SI Appendix, or Movies S1–S4.

**ACKNOWLEDGMENTS.** X.H. acknowledges the University of California, Los Angeles start-up funding, Air Force Office of Scientific Research Award FA9550-17-1-0311, and Office of Naval Research Award N00014-17-1-2117. S.W. acknowledges the support of the China Postdoctoral Science Foundation Grant (Grant 2019M651480).

1. T. Bartels-Rausch, Chemistry: Ten things we need to know about ice and snow. *Nature* **494**, 27–29 (2013).
2. C. C. Ryerson, Ice protection of offshore platforms. *Cold Reg. Sci. Technol.* **65**, 97–110 (2011).
3. M. Farzaneh, *Atmospheric Icing of Power Networks*, (Springer, 2008).
4. D. M. Ramakrishna, T. Viraraghavan, Environmental impact of chemical deicers—A review. *Water Air Soil Pollut.* **166**, 49–63 (2005).
5. N. Dalili, A. Edrisy, R. Carrievau, A review of surface engineering issues critical to wind turbine performance. *Renew. Sustain. Energy Rev.* **13**, 428–438 (2009).
6. O. Parent, A. Ilinca, Anti-icing and de-icing techniques for wind turbines: Critical review. *Cold Reg. Sci. Technol.* **65**, 88–96 (2011).
7. P.-O. A. Borrebaek, B. P. Jelle, Z. Zhang, Avoiding snow and ice accretion on building integrated photovoltaics—Challenges, strategies, and opportunities. *Sol. Energy Mater. Sol. Cells* **206**, 110306 (2019).
8. T. Wang *et al.*, Passive anti-icing and active deicing films. *ACS Appl. Mater. Interfaces* **8**, 14169–14173 (2016).
9. Y. Shen *et al.*, Icephobic materials: Fundamentals, performance evaluation, and applications. *Prog. Mater. Sci.* **103**, 509–557 (2019).
10. S. K. Thomas, R. P. Cassoni, C. D. MacArthur, Aircraft anti-icing and de-icing techniques and modeling. *J. Aircr.* **33**, 841–854 (1996).
11. L. Wang, Q. Gong, S. Zhan, L. Jiang, Y. Zheng, Robust anti-icing performance of a flexible superhydrophobic surface. *Adv. Mater.* **28**, 7729–7735 (2016).
12. Z. He *et al.*, Tuning ice nucleation with counterions on polyelectrolyte brush surfaces. *Sci. Adv.* **2**, e1600345 (2016).
13. J. Lv, Y. Song, L. Jiang, J. Wang, Bio-inspired strategies for anti-icing. *ACS Nano* **8**, 3152–3169 (2014).
14. M. J. Kreder, J. Alvarenga, P. Kim, J. Aizenberg, Design of anti-icing surfaces: Smooth, textured or slippery? *Nat. Rev. Mater.* **1**, 15003 (2016).
15. T. S. Wong *et al.*, Bioinspired self-repairing slippery surfaces with pressure-stable omniphobicity. *Nature* **477**, 443–447 (2011).
16. K. Rykaczewski, S. Anand, S. B. Subramanyam, K. K. Varanasi, Mechanism of frost formation on lubricant-impregnated surfaces. *Langmuir* **29**, 5230–5238 (2013).
17. J. Chen *et al.*, Superhydrophobic surfaces cannot reduce ice adhesion. *Appl. Phys. Lett.* **101**, 18–21 (2012).
18. S. Jung *et al.*, Are superhydrophobic surfaces best for icephobicity? *Langmuir* **27**, 3059–3066 (2011).
19. S. Dash, J. de Ruiter, K. K. Varanasi, Photothermal trap utilizing solar illumination for ice mitigation. *Sci. Adv.* **4**, t0127 (2018).
20. X. Yin *et al.*, Integration of self-lubrication and near-infrared photothermogenesis for excellent anti-icing/deicing performance. *Adv. Funct. Mater.* **25**, 4237–4245 (2015).
21. E. Mitridis *et al.*, Metasurfaces leveraging solar energy for icephobicity. *ACS Nano* **12**, 7009–7017 (2018).
22. C. Walker *et al.*, Transparent metasurfaces counteracting fogging by harnessing sunlight. *Nano Lett.* **19**, 1595–1604 (2019).
23. D. Wu *et al.*, Durable deicing lubricant-infused surface with photothermally switchable hydrophobic/slippy property. *Mater. Des.* **185**, 108236 (2020).
24. H. H. Richardson *et al.*, Thermo-optical properties of gold nanoparticles embedded in ice: Characterization of heat generation and melting. *Nano Lett.* **6**, 783–788 (2006).
25. L. Ma *et al.*, Plasmon-mediated photothermal and superhydrophobic TiN-PTFE film for anti-icing/deicing applications. *Compos. Sci. Technol.* **181**, 107696 (2019).
26. T. Cheng, R. He, Q. Zhang, X. Zhan, F. Chen, Magnetic particle-based superhydrophobic coatings with excellent anti-icing and thermoresponsive deicing performance. *J. Mater. Chem. A Mater. Energy Sustain.* **3**, 21637–21646 (2015).
27. G. Jiang, L. Chen, S. Zhang, H. Huang, Superhydrophobic SiC/CNTs coatings with photothermal deicing and passive anti-icing properties. *ACS Appl. Mater. Interfaces* **10**, 36505–36511 (2018).
28. M. R. Maghami *et al.*, Power loss due to soiling on solar panel: A review. *Renew. Sustain. Energy Rev.* **59**, 1307–1316 (2016).
29. X. Deng, L. Mammen, H. J. Butt, D. Vollmer, Candle soot as a template for a transparent robust superamphiphobic coating. *Science* **335**, 67–70 (2012).
30. W. Sun *et al.*, Water-dispersible candle soot-derived carbon nano-onion clusters for imaging-guided photothermal cancer therapy. *Small* **15**, e1804575 (2019).
31. L. Wang, T. J. McCarthy, Covalently attached liquids: Instant omniphobic surfaces with unprecedented repellency. *Angew. Chem. Int. Ed. Engl.* **55**, 244–248 (2016).
32. S. Wooh, H. J. Butt, A photocatalytically active lubricant-impregnated surface. *Angew. Chem. Int. Ed. Engl.* **56**, 4965–4969 (2017).
33. S. Wooh, N. Encinas, D. Vollmer, H. J. Butt, Stable hydrophobic metal-oxide photocatalysts via grafting polydimethylsiloxane brush. *Adv. Mater.* **29**, 1–7 (2017).

34. Z. Su, W. Zhou, Y. Zhang, New insight into the soot nanoparticles in a candle flame. *Chem. Commun. (Camb.)* **47**, 4700–4702 (2011).
35. Y. Takeuchi, Sagittal plane spinal mobility is associated with dynamic balance ability of community-dwelling elderly people. *J. Phys. Ther. Sci.* **29**, 112–114 (2017).
36. Y. Mastai, S. Polarz, M. Antonietti, Silica-carbon nanocomposites—A new concept for the design of solar absorbers. *Adv. Funct. Mater.* **12**, 197–202 (2002).
37. H. K. Raut, V. A. Ganesh, A. S. Nair, S. Ramakrishna, Anti-reflective coatings: A critical, in-depth review. *Energy Environ. Sci.* **4**, 3779–3804 (2011).
38. Y. Xu *et al.*, Icephobic behaviors of superhydrophobic amorphous carbon nanofilms synthesized from a flame process. *J. Colloid Interface Sci.* **552**, 613–621 (2019).
39. J. Liu *et al.*, Guided self-propelled leaping of droplets on a micro-anisotropic superhydrophobic surface. *Angew. Chem. Int. Ed. Engl.* **55**, 4265–4269 (2016).
40. P. Guo *et al.*, Icephobic/anti-icing properties of micro/nanostructured surfaces. *Adv. Mater.* **24**, 2642–2648 (2012).
41. J. Liu *et al.*, Distinct ice patterns on solid surfaces with various wettabilities. *Proc. Natl. Acad. Sci. U.S.A.* **114**, 11285–11290 (2017).
42. S. Peng *et al.*, Photocatalytically stable superhydrophobic and translucent coatings generated from PDMS-grafted-SiO<sub>2</sub>/TiO<sub>2</sub>@PDMS with multiple applications. *Langmuir* **35**, 2760–2771 (2019).
43. D. T. Eddington, J. P. Puccinelli, D. J. Beebe, Thermal aging and reduced hydrophobic recovery of polydimethylsiloxane. *Sens. Actuators B Chem.* **114**, 170–172 (2006).